Title Consequences of blindness for neural dynamics in mouse visual cortex

Authors Pouria Riyahi[1,2], Marnie A. Phillips[1], Nathaniel Boley[3] and Matthew T. Colonnese[1]

Affiliations

[1]The George Washington University
Department of Pharmacology and Physiology
Washington, D.C. 20052

[2]The George Washington University School of Medicine
Department of Biomedical Engineering
Washington, D.C. 20052

[3]The George Washington University School of Medicine
Institute for Biomedical Sciences
Washington, D.C. 20052

Abbreviated Title Blindness-induced changes in neural dynamics

Corresponding author colonnese@gwu.edu

Number of pages 36

Number of figures 8

Number of tables 3

Number of words:

Abstract 239

Introduction 641

Discussion 1473

Conflict of interest statement The authors declare no competing financial interests.

Acknowledgements

The authors thank Dr Mary Ann Stepp (GWU) for her guidance on corneal and lens health assays and ocular health assessment.

ABSTRACT

Early-life blindness causes lasting visual impairment, for which the circuit basis is only partially understood. Degradation of visual connections as well as the network dynamics supporting neural oscillations and arousal states are likely contributors. To define how blindness affects dynamics, we examined the effects of two forms of blindness, bilateral loss of retinal input (enucleation) and degradation of visual input (eyelid-suture), on emergent network properties and their state-dependence in the visual cortex of awake head-fixed mice. Neither form of early visual deprivation fundamentally altered the state-dependent regulation of firing-rates or local field potential oscillations. However, each form of deprivation did cause a unique set of changes in network behavior. Enucleation caused a loss of low-frequency synchronization specifically during movement, suggesting a mouse model for human alpha oscillations. Neurons were also less correlated and fired more regularly, with no change in mean firing rates. Chronic lid-suture decreased firing rates during quiet-wakefulness, but not during movement, and had no effect on neural correlations or firing regularity. Sutured animals also had a broadband increase in LFP power and increased occurrence, but reduced central frequency, of narrowband gamma oscillations. The complementary, rather than additive, effects of lid-suture vs.enucleation suggest that the development of these emergent network properties does not require vision but is plastic to modified input. Our results suggest that the etiology of human blindness will be a crucial determinant of circuit pathology and its capacity to respond to clinical interventions.

SIGNIFICANCE STATEMENT

Early life blindness alters brain circuits in a way that prevents a full return to normal vision even when sight is restored. We examined the circuit changes caused by two forms of blindness in the mouse as reflected in the spontaneous behavior (network dynamics) of the visual cortex. We found that, as in humans, vision is largely unnecessary for the establishment of cortical network dynamics and their modulation by cortical states like arousal. However, blindness did induce several important changes, such as loss of alpha rhythms. There was no overlap in the changes caused by each deprivation, suggesting that etiology matters. Understanding the lasting consequences of early blindness on neural function is essential for treatment of devastating early visual disorders.

INTRODUCTION

Blindness profoundly impairs visual processing even when sight is restored. This includes persistent deficits in shape recognition, contrast sensitivity, object representation, and visual scene integration (Fine et al., 2003; Kalia et al., 2014; Huber et al., 2015; McKyton et al., 2015, Mitchell and Maurer 2022). Understanding the circuit mechanism of these impairments is crucial if sight restoration is to be successful. Primate and clinical studies suggest early life blindness from all causes results in a remodeled visual cortex (Röder and Kekunnaya, 2022). The chronically blind visual cortex has more cross-modal inputs (Merabet and Pascual-Leone, 2010), increased blood flow and energy usage (Mishina et al 2003, Veraart et al., 1990), is more responsive to non-visual stimuli (Burton 2003), and lacks alpha oscillations(Adrian and Matthew, 1934; Jeavons, 1964; Noebels et al., 1978; Lubinus et al., 2021), with little effect on other frequencies (Hawellek et al. 2013). Changes in cortical processing associated with visual impairment are now understood to span both primary visual cortex as well as higher visual and non-visual brain regions (Guerreiro et al 2016, Mitchell and Maurer 2022).

In animals the structural and functional remodeling that occurs in visual cortex after binocular deprivation or denervation has been well studied (Huberman et al. 2008, Ribic 2020). The recurrent circuitry of cortex and thalamus and specialized inhibitory cell-types give rise to network dynamics such as neural oscillations that contribute to visual computations and the modulation of sensory input by arousal and attention (Uhlhaas et al., 2008) . The effect of blindness on intrinsic dynamics is thus crucial to understand, because it could explain a paradox in deprivation studies: Visual deficits following pattern vision loss are greater than would be predicted by deficits in the response properties of neurons alone (Maurer et al., 2007; Kiorpes, 2016).

Mice have become a viable model to study visual processing circuitry, including the complex network dynamics underlying arousal state (Niell and Scanziani, 2021). Head-fixed mice permitted to run display shifts in cortical activity similar to those of primates during shifts in attention (Harris and Thiele, 2011). These include suppression of large amplitude slow-waves and increased gamma band power, increased firing-rates, and visual-response gain with increasing arousal (McGinley et al., 2015). The initial emergence of mature network dynamics in thalamus and cortex occurs just before eye-opening (Colonnese, 2014; Murata and Colonnese, 2018) and is unaffected by enucleation (Riyahi et al., 2021). Neuronal firing-rates and gamma oscillations then undergo qualitative development in the 3rd and 4th postnatal weeks(Hoy and

Niell, 2015; Shen and Colonnese, 2016) that is delayed by dark-rearing (Chen et al., 2015). Slow-wave sleep is vision-dependent with a critical period that extends into adulthood (Miyamoto et al., 2003), but the effects of blindness on awake adult dynamics have not been thoroughly investigated.

Here we examine the effect of two models of early life blindness on the establishment and maintenance of cortical dynamics. Bilateral enucleation at P6 or P13 allows us to compare the effect of retinal input removal before and after the onset of mature dynamics (Riyahi et al., 2021), without the significant thalamic and cortical rewiring caused by earlier loss of retinal inputs in mice(Olavarria and Hiroi, 2003; Golding et al., 2014).. Binocular eyelid suture initiated before eye-opening deprives the animal of pattern vision and the ability to visually guide behavior, while preserving luminance detection and circadian rhythms (Kampf-Lassin et al., 2011), similar to bilateral cataracts. Our results support a remarkable resilience of visual circuit dynamics to lifelong visual deprivation, likely mediated by powerful mechanisms of synaptic and intrinsic homeostasis that regulate firing rates and higher-order interactions (Turrigiano, 2017; Wu et al., 2020) We also identify limits of homeostatic plasticity in the face of long-term changes in input activity. By identifying activity changes similar to those observed in the blind, we develop the mouse as a valid model for blindness induced changes in cortical processing.

Methods and Materials

Animal care. Animal care and procedures were in accordance with *The Guide for the Care and Use of Laboratory Animals*(NIH) and approved by the Institutional Animal Care and Use Committee at The George Washington University. Postnatal day(P)0 is the day of birth. C57BL/6 were obtained from Hilltop Lab Animals(Scottsdale, PA) as timed pregnant females, and kept in a designated, temperature and humidity-controlled room on a 12/12 light/dark cycle and examined once per day for pups. Large litters were reduced to 6-8 pups. Each litter was split approximately evenly into experimental or control animals, pups were not sexed, and all pups within the litter were used.

Surgical Procedures. For bilateral enucleations, carprofen (5 mg/kg) in saline was injected 1 hour prior to surgery to reduce pain and inflammation. Surgical anesthesia was induced with 3% isoflurane vaporized in 100% O_2, verified by toe-pinch and respiratory rate and effort, and thermal support provided during surgery. An incision was made in the eyelid (P6) and the globe

of the eye was removed using forceps. For older animals (P13), the eyelid attachment had thinned enough to enable manual opening of the eyelid with only light pressure. The eye socket was filled with sterile surgical foam (GelFoam) and the eyelid closed using a tissue adhesive (Vetbond). Pups were post-operatively monitored and received follow-up injections of carprofen daily for 2 days. Sham control littermates received identical treatment, including eyelid puncture with the tip of a suture needle, without enucleation or GelFoam. For bilateral eyelid suture, on P11 animals were anesthetized and prepared for surgery as above except that hair removal was also necessary. This was achieved by placement of Vetbond over all pups' eyelids 2-3 days prior to surgery. Dams remove the vetbond during grooming and this also removes the underlying hair without tearing or chemical burn of the delicate eye tissue. To suture the eyes, an incision was first made with iris scissors to separate the eyelid. The cut ends of the incision were opposed manually and the incision fixed using running horizontal mattress microsutures (AROSurgical T06A09N14-13) to bring the cut ends neatly together. In this way the eyelid suture is held in place long term by the healed incision, with the sutures serving to hold them together just until this point (dams remove sutures within days). Pups received follow-up analgesia and sham littermates were treated the same, as for enucleation. The mice were observed daily for signs of incomplete fusion and any pups with any eyelid opening were removed from the study. Eyes were dissected post-mortem and examined for lens and corneal clarity and found to be clear, albeit with some scar tissue formation under the healed incision. Corneas were also examined with fluorescein (2% sodium USP) to assay cornea health and no wounding was observed.

For headpost placement, carprofen(5 mg/kg) in saline was injected 1 hour prior to surgery to reduce pain and inflammation. Surgical anesthesia was induced with 3% isoflurane vaporized in 100% O_2, verified by toe-pinch and respiratory rate and effort, then reduced to 1.5-3% as needed by monitoring breathing and toe pinch response. An electrical heating pad(36°C) provided thermoreplacement. For attachment of the head-fixation apparatus, the scalp was excised to expose the skull, neck muscles were detached from the occipital bone, and the membranes were removed from the surface of the skull. Topical analgesic was applied to the incision(2.5% lidocaine/prilocaine mix, Hi-Tech Pharmacy Co., Inc., Amityville NY). The head-fixation apparatus was attached to the skull with grip cement(Dentsply, Milford DE) over Vetbond™ tissue adhesive(3M). The fixation bar consisted of a custom manufactured rectangular aluminum plate with a central hole for access to the skull. After placement, the animal was maintained with 0.5-1% isoflurane until the dental cement cured, after which it

recovered on a warming table. Pups were post-operatively monitored and received follow-up injections of carprofen daily for 2 days. On the 3rd-5th day following surgery they began habituation to the recording apparatus. Habituation consisted of two days of exposure to the recording apparatus. Animals were placed in fixation under isoflurane anesthesia and given 10(day 1) and 30(day 2) minute exposures after recovery from anesthesia, including visual stimulation as required.

In vivo electrophysiology. After two days of habituation the animals were placed in the setup as before, but a craniotomy and electrode placement was performed while under anesthesia. For the craniotomy, the skull was thinned using a surgical drill and small bone flaps were resected to produce a ~150-300 µm diameter opening. Monocular visual cortex was targeted by targeting the region with the least vascular density 1.5-2.5mm lateral and 0.0-0.5 mm rostral to lambda. All recordings were made using a single shank, 32 channel array arranged in two parallel lines of contacts(A1x32-Poly2-5mm-50s-177, NeuroNexus Technologies, Ann Arbor MI). The electrode penetrated the brain orthogonally to the surface and was advanced to a depth of 500-800µm using stereotaxic micromanipulator until the top channels touched the cerebral-spinal fluid. Isoflurane was withdrawn and the animal allowed to recover for 60 min before recordings. In the absence of visual stimulation the room was completely dark(<0.01 Lumens).

For the enucleation experiments animals were recorded for 30 min in the dark. For the eyelid suture experiments, animals received visual stimulation from an LED monitor centered 30 cm from the contralateral eye subtending 120 of the contralateral visual field. Visual stimuli were displayed using custom software in Matlab using PsychToolbox (Brainard, 1997; Pelli, 1997) . Stimuli consisted of 3 alternating blocks, each 60 secs and repeated for 30 min(10 exposures to each block). The blocks were “Black” consisting of total darkness, “Gray” consisting of a gray screen 130 Lumen/m^2 at the eye, and “Noise” with the same total luminance divided into blocks ~10 degrees of visual space randomly assigned to 0, 0.25, 0.5, 0.75 and 1 of the screen maximal luminance. The grids were updated at 5Hz. While total luminance was constant, local light intensity varied by +/-10 Lumens/m^2 with each grid change.

Data acquisition and analysis. Data was amplified 192V/V and digitized at 30 kHz on a SmartLink Headstage and recorded with the SmartBox 1.0(Neuronexus, Ann Arbor MI). Recordings were imported in Matlab using Neuronexus supplied macros and custom code. Depth(d)EEG signals were derived by down-sampling wide-band signals to 1 kHz after application of 0.1-350Hz zero-phase low-pass filter. For single-unit analysis channels with high

noise (outside the brain or bad contacts) were manually eliminated and the remaining channels saved as binary structures for spike sorting using Kilosort 1.0 (Pachitariu et al. 2016). Clusters were identified using the default parameters except ops.Th = [3 6 6]. Clusters were manually merged and sorted into noise, multi-unit and single-unit clusters using the GUI Phy (Rossant et al. 2016). Following sorting each good cluster was evaluated for inclusion as Regular or Fast-spiking using a modification of Vinck et al. (2015). Using the mean waveform, good clusters were separated using k-mean clustering based on normalized spike amplitude at 8/32 and 60/32 of a ms after the spike peak. The number of clusters was set to 3 and the two clusters with longest spikes were assigned to the regular spiking group and the other to the fast-spiking group.

All analyses were performed in Matlab. Spike-times were binned at 1 ms, and aligned with EEG signals. Animals were evaluated for inclusion based on the following criteria:(1) at least 10 well isolated 'good' units;(2) at least 10% and less than 50% time spent in movement condition,(3) local field potentials displaying normal relationships between layers, including elevated high(20+) frequency power relative to deep layers (Senzai et al., 2019),(4) absence of spreading depression and paroxysmal activity, (5) any evidence of eyelid separation for sutured animals. Spreading depression was identified as a sawtooth oscillation that spread slowly from surface to deep layers over 10-20 seconds and was followed by 1 or more minutes of silence. Paroxysmal activity was defined by the presence of 5 more seconds of high-amplitude(>3 fold above the maximal envelope for the remainder of the recording) spikes. In total 15/48 animals were eliminated from the enucleated experiment (9/19 sham; 6/29 Enucleated); and 12/29 animals(5/12 sham; 7/17 sutured) were eliminated from the suture experiments.

For analysis, recordings were divided into 500ms windows and the maximum velocity of the treadmill, firing rates for all neurons(expressed in Hz) and spectra of the LFP for the channel in layers 2-3 with the least artifact and maximals signal power were calculated. Spectral decomposition of the dEEG signal used the multi-taper method (Mitra and Bokil 2007) using a time-bandwidth product 3 and number of tapers 5. Spectral power was whitened by multiplication of power by frequency. Each 500ms window was sorted into Moving and Stationary conditions based on the presence or absence of movement of the circular treadmill. Mean spectra for each animal were calculated for Moving and Stationary periods, as were mean firing rates for each neuron. Spiking regularity(LvR) was calculated by the method of Shimomoto et. al.(2009) for each cluster across the entire recording. Calculation of spike-rate covariance followed the method of Renart et al.(2010). Each single-unit raster was convolved by a

normalized kernel that was the sum of a rapid time-window(J) and a negative longer window(T, 4xJ). All analysis except for the effect of J(Fig. 7F), was made with J=160ms. For the isolation of 3-5Hz oscillations we identified periods of high amplitude negative potentials in which at least 3 peaks > 3 standard deviations below the mean negative potential occurred within 1 s. These periods were further restricted to require at least 20 ms with no spiking(combined multi and single unit) between each high-amplitude spike. This method was most consistent with identifying all periods of visible 3-5Hz oscillation occurring after movement.

Statistical Procedures. All data are mean ± SEM except for the cumulative distributions of spike rates which are 95% confidence intervals and the means of firing rates which are standard deviation. The statistical test applied is noted along with results. Statistical tests were applied in Matlab using the inbuilt functions('ttest2', 'anovan'). Significance statements regarding normalized frequency power distributions were calculated by permutation analysis following the permutation test method of Cohen(2014), using custom macros. Frequency resolution was 1 Hz from 1-100 Hz. The significance threshold was $p<0.05$.

Results.

Effects of enucleation on cortical dynamics.

To examine the requirement for the primary sensory input in establishing and calibrating neural network dynamics of visual cortex, we made acute recordings of the local field potentials (LFP) and action potentials extracellularly using single shank polytrodes from the contralateral monocular region of primary visual cortex of awake, head-fixed adult mice. The mice were divided into four groups: P6 enucleated(EN6, n=13) and their Sham surgery littermate controls(n=5), and P13 enucleated(EN13,n=10) and their Sham littermate controls(n=5)(Fig. 1A). No significant(P>0.5 for all comparisons) or visible differences were observed for any measurement between the two sham groups and they were consolidated into a single Sham control group for analysis. To examine the state-dependence of cortical dynamics, recordings were performed while the mice were allowed free movement on a circular treadmill. To equalize the visual input to the groups, all recordings were performed in complete darkness(Fig. 1A).

To quantify the behavior of the cortical circuit we used two primary measures: (1) local field potentials from layer 4, which are most revealing of both the low and high-frequencies that

define behavioral state(Senzai et al., 2019) and (2) action potentials sorted into single-unit clusters throughout the depth of cortex. Because of variability in the absolute depths of the recordings and ambiguity in assigning layers across very different experimental conditions, single units were not divided by layer. Single-unit clusters were divided into regular and fast-spiking units by conventional means (Vinck et al., 2015).

Qualitatively, enucleation at either age did not change the patterns of cortical network activity visible on a treadmill (Fig. 1B-C). EN6 and EN13 animals both exhibited spontaneous background activity in the dark that was similar to the Sham control and to that described previously for head-fixed mice(Cardin et al., 2009; Niell and Stryker, 2010). Specifically, periods with no movement (Stationary) were dominated by large amplitude, synchronous, slow (below 10Hz) fluctuations of the LFP and neural firing. Periods of movement were associated with an increase in neural firing rates, a reduction of the firing-rate variance, and a decrease in the total LFP amplitude reflecting a drop in low frequencies and an increase in high frequencies (20 + Hz). Visual observation of multiple animals suggested two differences between enucleated and control animals: 1) The low amplitude, high-frequency LFP observed during movement was flatter and more consistent in enucleated animals, and 2) Many enucleated animals had an increased incidence and size of very high amplitude 3-5Hz oscillations that followed the cessation of movement (Fig. 1C).

To quantify the LFP modulation by state we calculated frequency power for the upper layers in one second windows, divided into Stationary and Moving periods based on the treadmill velocity(Fig. 2A). During Stationary periods the LFP power was not significantly different between groups for any frequency. During Moving periods both EN6 and EN13 displayed significantly lower power from 4 to 22Hz (24Hz for EN6) compared to Sham, confirming our visual impression that the LFP flattens more during movement in enucleated animals. To examine the effect of movement on LFP power we calculated the proportional change for each frequency band during Moving periods with Stationary periods as baseline. This analysis showed a significantly greater decrease (or reduced increase for frequencies above 20Hz) in frequency power between 2 and 26 Hz for EN6 and between 2 and 36 Hz for EN13. In total these data suggest that regulation of cortical excitability by arousal and movement (Vinck et al., 2015) is not altered by enucleation occurring either before these circuits develop (EN6) or immediately after they emerge (EN13). However, in the absence of the eyes, movement has an increased effect in suppressing low-frequency oscillations. This reduction in low-frequency

power was limited to movement periods, and was not present when these rhythms are most prevalent, during Stationary periods.

To determine if enucleation changed neuronal behavior, we sorted spikes in presumptive single-units and divided the isolated units into regular-spiking (presumed excitatory) and fast-spiking (presumed inhibitory) clusters. Firing-rate distributions and means were compared for each group(Fig. 2B & C). For regular-spiking neurons a two-factor ANOVA for group and movement state revealed significant effects for both group and movement but no interaction between the groups (Table 1). The group effect likely results from a decrease in mean firing rates for both EN6 and EN13 present for both Stationary and Moving conditions. However, post-hoc tests did not show a significant difference between sham and experimental conditions for the separate Stationary or Moving conditions. Post-hoc analysis confirmed that movement was associated with an increase in firing-rates for all experimental conditions. The amplitude and distribution of movement modulation was not significantly different for regular spiking neurons in either EN6 or EN13. Fast-spiking neurons showed a significant effect of movement by 2-factor ANOVA, but no effect of group or interaction between group and movement. Similarly the degree of movement modulation was not significantly different for each of the groups. These results show that enucleation(either at P6 or P13) causes a moderate reduction in fast-spiking neuron firing rates across behavior states, but does not affect the regulation of firing by movement. They confirm results in animals in which pupil dilation can be directly monitored to measure arousal separately from movement (Vinck et al., 2015), that the modulation of the LFP and the increased firing-rates are dissociable and show that enucleation only strongly affects the LFP.

Role of pattern visual experience in cortical dynamics

Enucleation eliminates the retina, depriving the visual system of both visual experience and spontaneous activity critical for circuit formation and maintenance(Hooks and Chen, 2020). To examine the effects of visual, rather than retinal, deprivation on the establishment of cortical dynamics and to more closely model reversible pattern vision loss by cataracts, we bilaterally sutured the eyelids before natural eye-opening (Sutured group, n=10), and compared them to littermates undergoing a Sham surgery (n=7) on the same day. Eye closure was maintained through the recording period (i.e. the animals were recorded with the eyes sutured) to directly compare with the blind and with the enucleation experiments. For the eye-suturing experiments the animals faced an LED screen targeted at the contralateral eye (Fig. 3A). Visual stimulation

consisted of 1 min blocks of a black screen to test spontaneous activity in the dark, a gray screen to examine low-contrast luminance responses (a visual stimulus likely perceived similarly by the two groups), and an equiluminant ‘noise’ stimulus consisting of randomly shifting changes in luminance of large squares which should be visible only to the open eyes of the Sham animals.

Like the enucleated animals, the gross neural behavior in the visual cortex was qualitatively similar in Sutured and Sham control animals(Fig. 3B). Visual inspection suggested a strong increase in firing during Noise blocks in Sham animals that was not present in Sutured littermates, while both groups showed strong increases in firing during moving periods in all stimuli conditions. Sutured animals were very likely to display prominent narrow-band gamma power increases during both Gray and Noise blocks, while this narrow band oscillation was present in fewer than half of Sham animals and only during the Gray screen blocks.

We first quantified the behavior of the layer 4 LFP. In the dark, Sutured animals displayed a broad-band increase in frequency power that was present during both Stationary and Moving periods(Fig 4A). This increase was significant for the frequencies 2-28Hz during Stationary and 2-56Hz & 70-78Hz for Moving periods. The modulation of the LFP power by movement was largely similar between groups, but there was a significant difference between 14-24Hz.

During Gray screen blocks both groups displayed a prominent peak in the spectra resulting from narrowband gamma activity. The frequency of the peak was shifted to lower frequencies in Sutured animals(peak 64-66Hz in Sham and 56-58Hz in Sutured). Overall power was higher for sutured animals 2-28Hz & 52-54Hz during Stationary and 2-60Hz, 74-80Hz & 84-92Hz during Moving. Both groups had a similar decrease in low frequency and increase in high-frequency power during movement, but Sutured animals showed a significantly greater increase in the narrowband gamma power(54-64Hz) during movement. We quantified the effect of visual stimulation by calculating the proportional change between Black blocks and Gray blocks during Stationary and Moving periods(Fig. 4B). The only significant modulation of the LFP by Gray-screen was an increase in narrow-band gamma power, an increase that was greater during movement. This frequency of this shift was lower for Sutured animals both for Stationary and Moving conditions (significant differences at 52-54Hz with no difference in amplitude) and with a great amplitude during Movement (significant difference in power 54-60Hz during Movement).

Noise stimulation blocks caused the wideband power differences between Sham and Sutured animals to disappear and differences between the two groups became largely limited to beta and gamma band powers. During Stationary periods the differences between the two groups was limited to the 2-4 & 50-60Hz bands. The later gamma frequency differences reflect the suppression of suppressed narrowband gamma in Sham but not Sutured animals, consistent with its origins as a contrast-suppressed luminance activity generated in the retina (Saleem et al., 2017; Storchi et al., 2017). During Movement, Sutured animals had significantly higher power across the broad range of beta-gamma frequencies (18-60Hz). This shift was reflected in modulation by movement during noise. Sutured animals had increased suppression of low frequencies (2-10Hz) and increased amplification of high-frequencies (22-66 Hz) during Movement. As suggested by the raw spectra, the effect of patterned visual stimulation was very different between groups. Compared to the frequency powers present in the dark (black screen), Sham animals showed large power increases below 20Hz and above 60Hz during noise stimuli (Fig. 4B right) during both Stationary and Moving periods (significance points not shown). In contrast, the stimulus-driven increases in low and very high frequencies were moderate or absent in the Sutured animals (reduced modulation 2-20 & 72-100Hz Stationary and 8-10 & 74-86Hz Moving). Instead, Sutured animals showed a greater increase in stimulus driven narrow-band gamma power (52-60Hz) while Stationary, and narrow-band gamma plus lower beta-gamma powers (22-64Hz) while Moving. Overall, the LFP data show a broadband increase in LFP power, and normal regulation of the oscillatory regime by state in sutured animals. In addition, sutured animals appear to have increased sensitivity or capacity to generate narrowband gamma oscillations in response to low-contrast luminance. Not surprisingly, Sutured animals generate narrowband gamma activity in response to high-contrast noise stimuli, as this stimulus is filtered by the sutured eyelids, while Sham animals show suppression of narrowband gamma. The origin of the increase in low frequency activity by Noise stimuli in sighted animals is harder to understand, but is a likely combination of the update rate (5 Hz) and intrinsic dynamics. This is lower in the Sutured animals as they have reduced luminance and contrast on the retina.

Neuronal firing rates were also altered by chronic eye closure, with stronger effects observed for regular spiking neurons(Fig. 5 & 6; Table 2 & 3). Population means for firing rates were analyzed by 3-factor ANOVA(experimental group vs. move condition vs. stimulation block), which showed significant effects for each factor and an interaction between group and movement condition. Examination of the post-hoc tests and firing-rate distributions suggest that

these differences result from a decrease in firing-rates for Sutured animals during Stationary periods in all stimulus conditions(Fig. 5A left). Interestingly, firing-rates became similar during Moving periods, again for all stimulus conditions(Fig. 5A center column). This normalization of firing-rates during movement periods implies the firing-rate increases occurring during movement should be greater in Sutured animals(Fig. 5A right column). 2-factor ANOVA for group and stimulation block revealed an effect of group on mean firing-rate modulation, but not an effect of stimulus block or interaction of the two. In all stimulus conditions sutured animals had larger mean firing rate increases during movement, but this was significant only for the dark blocks. Examination of firing-rate as a function of stimulus condition showed strong increases in firing-rates driven by the noise stimulus block, but not for the gray screen blocks in the sham treated animals(Fig. 5B). This increased firing by noise stimulus was not present in the Sutured animals. As a result the firing-rate modulation index for noise stimulation was significantly lower in sutured animals during both Stationary and moving periods, likely reflecting the lack of patterned vision through their closed eyelids.

The behavior of fast-spiking, presumptive interneurons, was not strongly affected by eye closure. Mean firing rates and distributions were similar between experimental groups for all behavioral and stimulation conditions(Fig. 6A; Table 2). Likewise, movement modulation was similar in both groups. As was observed for regular spiking neurons, neuron firing rates increased by noise stimuli only for Sham animals and therefore the modulation by noise stimulus was significantly lower for the Sutured animals, likely reflecting their lack of patterned vision(Fig. 6B).

Overall our results confirm that eyelid suture obscures pattern vision, as reflected in a loss of LFP and spiking responses to the noise stimulus condition. We observed a continued presence of narrow-band gamma following visual deprivation. The sensitivity of narrow-band gamma likely increased following eyelid suture as the oscillations were more prevalent during gray screen stimuli despite the attenuation of the closed eyelid. Finally we observed a reduction in excitatory neuron firing rates during a period of quiet wakefulness that was not due to reduced sensory drive.

Role of visual and retinal experience in establishing higher-order neuron behavior.

Beyond firing rates, we quantified regularity of neuron firing and the pairwise neural firing rate correlations, parameters that have been shown to differentiate cortical regions and be homeostatically regulated(Hengen et al., 2013; Mochizuki et al., 2016; Wu et al., 2020). To quantify firing pattern we adopted a metric of variance for interspike-interval(LvR) that is independent of firing rate and reveals differences in firing patterns between primate cortical regions(Shinomoto et al., 2009). Regular firing generates a low(<1) LvR, and bursty neurons a high(2+) LvR. Enucleation at P6 and P13 altered the regularity of neuron firing, and neurons became more regular than Sham controls(Sham 1.31± 0.30(StDev), EN6 1.25±0.32, EN13 1.20±0.31; ANOVA F=5.46 p=0.004)(Fig. 7A). Eye-suturing, however, did not significantly change the distribution or mean regularity of neurons(1.35±0.31 vs 1.32±0.36, t-test p = 0.32)(Fig. 7B).

Visual deprivation disrupts the refinement of horizontal connections that link cortical neurons with similar receptive fields(Huberman et al., 2008). However this shift occurs as a rearrangement of neuronal connections, largely keeping the connection probabilities constant(Ko et al., 2013). To determine if local connections and the resultant correlation between neuron pairs is changed following deprivation, or if it is under long-term homeostatic control as observed for short term correlation during juvenile development(Wu et al., 2020), we calculated pairwise firing-rate covariance for all the single-units isolated in individual animals. The mean pairwise correlation for each animal was then used to compare the experimental groups to their respective controls. As we did not observe any differences between EN6 and EN13 we combined these groups for the analysis. Mean pairwise covariance was similar between the Sutured and Sham controls, but was significantly reduced in Enucleated animals compared to their Sham control(Fig. 7A)(Suture Control: 0.065±0.001(SEM); Sutured: 0.057±0.011; Enucleation Control:0.069±0.014; Enucleated: 0.035±0.003)(ANOVA F=4.71; p = 0.0059, with significant differences between the Enucleated and Sham-Enucleated groups only). We asked whether the correlation difference in the enucleated experiment were specific to the Stationary or Moving period(Fig 7B). Mean pairwise correlations showed a significant effect for both experimental group and state but no interaction between the two(Sham Stationary 0.069±0.014; En Stationary 0.035±0.003(SEM); Sham Moving 0.029±0.007; En Moving 0.013±0.002; 2-factor ANOVA F=18.4, p = 0.0001 for group; F=27.14 p = 0.000002 for state; F= 2.5 p = 0.1185 for interaction). Post-hoc tests show significant mean differences between control and experimental groups for both Stationary and moving conditions. Thus lower correlations may result from underlying loss of connections rather than changes to the dynamics

of either state. Finally, to determine if the lower correlation in enucleated animals is specific to the time window used for correlation calculation, we calculated correlations for multiple windows from 20 to 320 ms(Fig. 7C). We observed lower correlations for all window sizes that increased with the size of the window(ANOVA for effect of group: F=31.46 p = 6.79*10-8; effect of window size F=31.76 p = 1.09*10-23; interaction F=2.47 p=0.033).

Our results show a more profound effect of enucleation on higher-order behavior of neurons, increasing the regularity and decreasing pairwise correlations. In contrast, visual deprivation did not change these behaviors, though it caused a reduction in neuron firing rates.

Role of retinal experience in the development of 3-5 Hz 'alpha' rhythms

Headfixed mice frequently display a prominent slow oscillation immediately upon cessation of movement. This so-called '3-5Hz oscillation' shares similarities in the pattern of thalamic and cortical engagement with the human alpha rhythm (Senzai et al., 2019; Nestvogel and McCormick, 2022). Our initial visual inspection of enucleated and sutured animals indicated no loss of the 3-5 Hz Stationary rhythm; rather the rhythm appeared more prominent particularly in enucleated animals. Such an increase might be expected if corticothalamic connections are strengthened by enucleation as they are in mice with disrupted retinal development(Seabrook et al., 2013). In our set-up the peak in LFP frequency power for this rhythm was closer to 5-8 Hz which largely reflected the frequencies in the individual LFP spikes, rather than the inter-trough intervals, which were closer to the 3-5Hz described by others. We did not observe a significant change in these frequencies for the non-moving conditions in enucleated animals, suggesting no major regulation of the 3-5Hz pattern. However, any changes may have been masked by the long Stationary periods that did not show the oscillation. In sutured animals we did observe an increase in power at the relevant frequencies, but this increase occurred as part of a wide-band increase in frequency power that was also present during movement.

To directly test the effects of enucleation on the 3-5Hz oscillation we isolated periods of this oscillation from the remainder of the Stationary periods. The spectra of neither enucleated group showed any significantly different frequencies from control for either the isolated periods of 3-5Hz oscillation, nor for the remainder of the Stationary periods(Fig. 8A). However, enucleated animals did have an increase in the occurrence of the oscillations(Fig 8B). Periods of 3-5Hz oscillation occupied 2.14±0.39%(SEM) of the recording for sham animals, 3.05±0.39% in E6

animals and 4.19±0.47% in E13 animals(one-way ANOVA for group F=4.5 p=0.013, with sham significantly different from E13 by post-hoc test). Sutured animals, in contrast, showed increased frequency power during 3-5Hz episodes (significant bands: 2-10, 14-15, 18-20, 24, 28-29Hz). Interestingly, removing the 3-5Hz periods eliminated the significance differences in the spectra for the remainder of the Stationary period(Fig 8C). There were no differences between groups in the incidence of 3-5Hz oscillations(Sham 2.51±0.40% vs Sutured 2.13±0.40%, t-test F-0.42 p=0.53)(Fig. 8D).

In sum, our data show that the development of the large amplitude 3-5Hz inactivation rhythms does not depend on retinal input nor patterned visual input to thalamus. Absence of these inputs actually increases their incidence or amplitude depending on the form of deprivation.

Discussion

We used extracellular polytrode recordings of ongoing background activity in awake, headfixed adult mice allowed to run freely on a treadmill to explore how two models of blindness in mice modify the activity dynamics of visual cortex. While many aspects of cortical dynamics, including state-dependence, are qualitatively normal following chronic deprivation, blindness did induce a number of persistent quantitative changes, including a loss of alpha-beta similar to that observed in congenital blindness in humans (Hawellek et al., 2013; Lubinus et al., 2021). Surprisingly, the effects of each form of blindness were complementary, not additive. Enucleation primarily altered cortical network properties including cortical oscillations, correlations and firing patterns, with only a moderate effect on firing rates. In contrast, eyelid suture reduced firing rates of excitatory neurons but left other properties largely intact. Our findings suggest that the establishment and maintenance of cortical network properties is largely independent of activity in the primary sense organ. However, changes in input and activity do influence the development of alpha-oscillations as well as influencing homeostatic set-points for neuronal firing rates and higher-order network interactions.

Cortical 'alpha' and blindness

Alpha and beta frequencies were suppressed in enucleated, but not sutured, animals. This is consistent with reports of occipital alpha loss in congenitally blind individuals, particularly in those with more severe vision loss (Jan and Wong, 1988; Bottari et al., 2016). Posterior alpha is present early (Campus et al., 2021), suggesting a regressive process disassembles alpha generators in the absence of light in the blind. Loss of alpha and beta was specific to

movement periods, when low-frequency (delta and alpha) activity is already low (Niell and Stryker, 2010). Our results do not support a homology between human alpha and the bursts of 3-5 Hz activity prevalent just after movement periods in mice. This homology is based on electrophysiological similarities of these rhythms (Senzai et al., 2019; Nestvogel and McCormick, 2022) and a similar correlation with pupil dilation during quiet-waking(Reimer et al., 2014; Montefusco-Siegmund et al., 2022), though the temporal relationship between pupil dilation and low-frequency/alpha power is different in humans and rodents (Montefusco-Siegmund et al., 2022). Rather than loss, we observed increased post-movement 3-5Hz bursts in both blindness models, and Reimer et al. (2014) observed no loss of similar oscillations after retinal degeneration. If the 3-5Hz bursts are indeed mouse alpha, then their development is not dependent on visual transduction like human alpha. If, on the other hand, mice and humans have similar visual-dependent cortical rhythms, our data suggest that the low and medium frequencies that remain during movement and arousal (Einstein et al., 2017) may be the mouse form of alpha. The 3-5 Hz oscillations occurring during quiet wakefulness are likely homologues of human delta1/2 (0.5-4 Hz) which have increased power in blind adults and infants (Campus et al., 2021), similar to the increase in low frequencies observed in enucleated mice in the third postnatal week (Riyahi et al., 2021). The role of alpha and other frequencies in the loss and recovery of visual processing following cataract reversal is unclear (Bottari et al., 2016), but our results suggest ways to tractably study them in an animal model.

Homeostasis and circuit changes in blindness

Single neuron firing rates as well as higher-order network behaviors are homeostatically regulated in mouse visual cortex, returning to normal levels within days of manipulations that reduce or increase firing (Hengen et al., 2016; Wu et al., 2020; Torrado Pacheco et al., 2021). Our results indicate that, while clearly a powerful–even dominant–influence, intrinsic homeostatic set-points can be altered or overwhelmed by the profound changes in excitatory and inhibitory circuits resulting from visual deprivation(Ribic, 2020). While early loss of retinal input is associated with an occipital seizure focus(Kellaway, 1975), we did not observe seizure generation in any treatment group, and only a very moderate effect of lifelong visual and retinal deprivation on firing rates. Enucleation at P6, when spontaneous firing rates are approximately 10% that of adults (Riyahi et al., 2021), did not significantly change adult firing rates, suggesting that homeostatic set-points are determined centrally and independently of input. Unexpectedly, binocular deprivation–a procedure that causes less acute reduction in firing-rates and allows for more complete homeostatic plasticity in adults (Hengen et al., 2013; Keck et al., 2013) --did

lower firing-rates, but only during Stationary periods. It is unclear whether mean firing-rates were truly lower in sutured animals and an increased movement-related signal normalized them, or whether the firing-rate set points are similar in both animals but set in a state similar to our movement period. Firing-rate 'upscaling' following monocular deprivation occurs during wake (Hengen et al., 2016) suggesting this may also be a critical state in determining when the neuron has returned firing rates back to its setpoint.

Higher-order network behaviors such as pairwise correlation, firing regularity and network excitability are also rapidly altered by visual deprivation, but recover in an apparently homeostatic manner (Hengen et al., 2013; Ma et al., 2019; Wu et al., 2020). Each recovers on different timescales, likely because they depend on different homeostatic plasticity mechanisms (Keck et al., 2017). Our data support this, as pairwise correlations and firing regularity changed in enucleated animals despite similar-firing rates, while eyelid-suture reduced firing rates without changing correlation or regularity. Horizontal connections are selectively formed between neurons with similar visual response properties through a synaptic rearrangement that maintains the connection probability of the network (Ko et al., 2013). Significant numbers of correlated neurons are first observed around P15, after the times of enucleation here (Colonnese et al., 2017). Our data suggest that even though the level of correlation within the cortical network is largely intrinsically determined, it is developmentally influenced by the changes in activity following loss of retinal input, but not those following pattern vision loss. The same rules may apply to spiking regularity. An open question is whether changes in these network properties are the result of cross-modal input plasticity or the simple absence of retinal input. Spike intervals are more regular in 'higher-order' structures (Shinomoto et al., 2009), which receive a larger portion of their input from within the thalamocortical loop, and bilateral enucleation increases thalamocortical and cortico-cortical connections in opossums (Karlen et al. 2006). Thus strengthened corticothalamic input may underlie the increased regularity in enucleated animals, making V1 more like 'higher' cortex.

Cortical gamma oscillations and visual experience.

Narrowband cortical activity is generated in the retina to low-contrast luminance while broadband activity is generated in cortex in response to high-contrast, structured stimuli (Saleem et al., 2017; Veit et al., 2017; Storchi et al., 2017). Together these activities encode contrast and reflect multiplexed visual channels (Meneghetti et al., 2021). We observed an increase in both types following visual deprivation, but not after enucleation. Narrowband

gamma occurred at lower frequency but higher power in sutured animals. Narrowband gamma emerges during the fourth week with a central frequency around 52Hz, a process dependent on visual experience(Chen et al., 2015). Our data indicate extended visual deprivation does not prevent development of narrowband gamma, but does prevent an increase in its central frequency with age. In fact, pattern deprivation appears to increase sensitivity, as the luminance levels through the closed eyelids of the sutured animals are lower than controls, but have larger and more prevalent gamma oscillations during both low and high-contrast stimuli. This may reflect the persistent drive of diffused light through the closed eyelids, which reduced high-contrast specificity of the wideband oscillations as well as increased transmission through thalamus and cortex. Both enucleation and suture disrupt the development of cortical inhibitory circuits (Ferrer and De Marco Garcia, N V, 2022), so the normal-to-enhanced power of wideband gamma dependent on intracortical inhibition is unexpected. It is likely that homeostatic balancing of excitatory and inhibitory synapses can compensate to allow interneurons to synchronize the network with reduced absolute inhibition. Sutured animals did have an apparent increase in visually evoked narrow-band gamma oscillations despite the closed eyelids. With the exception of this gamma activity, blindness induced changes are likely the outcome of central circuit differences, and not an artifact of lack of vision, as the changes were observed even in the dark.

Conclusions

Our results add to an extensive human literature indicating that the blind visual cortex is remarkably functional despite failure of the normal visual processing circuitry to form (Burton, 2003; Kupers and Ptito, 2011). Regardless of the cause, visual deprivations had little to no effect on the state-dependent regulation of background activities, suggesting that generative mechanisms of important cortical behaviors such as slow-waves, asynchronous active states and beta-gamma oscillations are under homeostatic regulation and independent of input. We confirmed that the mid-frequency network oscillations involved in attention and long-range integration of vision are most susceptible to deprivation. These discrete pathologies may contribute to continued visual impairment following blindness reversal (Maurer et al., 2007; Kalia et al., 2014; Röder and Kekunnaya, 2022).

REFERENCES

Adrian ED, Matthew BHC (1934) The berger rhythm: Potential changes from the occipital lobes in man. Brain 57:355-385.

Bottari D, Troje NF, Ley P, Hense M, Kekunnaya R, Röder B (2016) Sight restoration after congenital blindness does not reinstate alpha oscillatory activity in humans. Sci Rep 6:24683.

Brainard DH (1997) The psychophysics toolbox. Spat Vis 10:433-436.

Burton H (2003) Visual cortex activity in early and late blind people. J Neurosci 23:4005-4011.

Campus C, Signorini S, Vitali H, De Giorgis V, Papalia G, Morelli F, Gori M (2021) Sensitive period for the plasticity of alpha activity in humans. Dev Cogn Neurosci 49:100965.

Cardin JA, Carlen M, Meletis K, Knoblich U, Zhang F, Deisseroth K, Tsai LH, Moore CI (2009) Driving fast-spiking cells induces gamma rhythm and controls sensory responses. Nature 459:663-667.

Chen G, Rasch MJ, Wang R, Zhang XH (2015) Experience-dependent emergence of beta and gamma band oscillations in the primary visual cortex during the critical period. Sci Rep 5:17847.

Colonnese MT (2014) Rapid developmental emergence of stable depolarization during wakefulness by inhibitory balancing of cortical network excitability. J Neurosci 34:5477-5485.

Colonnese MT, Shen J, Murata Y (2017) Uncorrelated neural firing in mouse visual cortex during spontaneous retinal waves. Frontiers in Cellular Neuroscience 11:289.

Einstein MC, Polack P, Tran DT, Golshani P (2017) Visually evoked 3-5 hz membrane potential oscillations reduce the responsiveness of visual cortex neurons in awake behaving mice. J Neurosci 37:5084-5098.

Ferrer C, De Marco Garcia, N V (2022) The role of inhibitory interneurons in circuit assembly and refinement across sensory cortices. Front Neural Circuits 16:866999.

Golding B, Pouchelon G, Bellone C, Murthy S, Di Nardo AA, Govindan S, Ogawa M, Shimogori T, Luscher C, Dayer A, Jabaudon D (2014) Retinal input directs the recruitment of inhibitory interneurons into thalamic visual circuits. Neuron 81:1057-1069.

Harris KD, Thiele A (2011) Cortical state and attention. Nat Rev Neurosci 12:509-523.

Hengen KB, Torrado Pacheco A, McGregor JN, Van Hooser SD, Turrigiano GG (2016) Neuronal firing rate homeostasis is inhibited by sleep and promoted by wake. Cell 165:180-191.

Hengen KB, Lambo ME, Van Hooser SD, Katz DB, Turrigiano GG (2013) Firing rate homeostasis in visual cortex of freely behaving rodents. Neuron 80:335-342.

Hooks BM, Chen C (2020) Circuitry underlying experience-dependent plasticity in the mouse visual system. Neuron 107:986-987.

Huberman AD, Feller MB, Chapman B (2008) Mechanisms underlying development of visual maps and receptive fields. Annu Rev Neurosci 31:479-509.

Jeavons PM (1964) The electro-encephalogram in blind children. Br J Ophthalmol 48:83-101.

Kalia A, Lesmes LA, Dorr M, Gandhi T, Chatterjee G, Ganesh S, Bex PJ, Sinha P (2014) Development of pattern vision following early and extended blindness. Proc Natl Acad Sci U S A 111:2035-2039.

Kampf-Lassin A, Wei J, Galang J, Prendergast BJ (2011) Experience-independent development of the hamster circadian visual system. PLoS One 6:e16048.

Keck T, Hubener M, Bonhoeffer T (2017) Interactions between synaptic homeostatic mechanisms: An attempt to reconcile BCM theory, synaptic scaling, and changing excitation/inhibition balance. Curr Opin Neurobiol 43:87-93.

Keck T, Keller GB, Jacobsen RI, Eysel UT, Bonhoeffer T, Hubener M (2013) Synaptic scaling and homeostatic plasticity in the mouse visual cortex in vivo. Neuron 80:327-334.

Kellaway P (1975) Afferent input: A critical factor in the ontogenesis of brain electrical activity. In: Behavior and brain electrical activity Afferent input: A critical factor in the ontogenesis of brain electrical activity. pp391-420.Springer.

Kiorpes L (2016) The puzzle of visual development: Behavior and neural limits. J Neurosci 36:11384-11393.

Ko H, Cossell L, Baragli C, Antolik J, Clopath C, Hofer SB, Mrsic-Flogel TD (2013) The emergence of functional microcircuits in visual cortex. Nature 496:96-100.

Kupers R, Ptito M (2011) Insights from darkness: What the study of blindness has taught us about brain structure and function. Prog Brain Res 192:17-31.

Lubinus C, Orpella J, Keitel A, Gudi-Mindermann H, Engel AK, Roeder B, Rimmele JM (2021) Data-driven classification of spectral profiles reveals brain region-specific plasticity in blindness. Cerebral Cortex 31:2505-2522.

Ma Z, Turrigiano GG, Wessel R, Hengen KB (2019) Cortical circuit dynamics are homeostatically tuned to criticality in vivo. Neuron 104:655-664.e4.

Maurer D, Mondloch CJ, Lewis TL (2007) Effects of early visual deprivation on perceptual and cognitive development. Prog Brain Res 164:87-104.

McGinley MJ, Vinck M, Reimer J, Batista-Brito R, Zagha E, Cadwell CR, Tolias AS, Cardin JA, McCormick DA (2015) Waking state: Rapid variations modulate neural and behavioral responses. Neuron 87:1143-1161.

Mochizuki Y et al (2016) Similarity in neuronal firing regimes across mammalian species. J Neurosci 36:5736-5747.

Murata Y, Colonnese MT (2018) Thalamus controls development and expression of arousal states in visual cortex. J Neurosci 38:8772-8786.

Nestvogel DB, McCormick DA (2022) Visual thalamocortical mechanisms of waking state-dependent activity and alpha oscillations. Neuron 110:120-138.e4.

Niell CM, Scanziani M (2021) How cortical circuits implement cortical computations: Mouse visual cortex as a model. Annu Rev Neurosci 44:517-546.

Niell CM, Stryker MP (2010) Modulation of visual responses by behavioral state in mouse visual cortex. Neuron 65:472-479.

Noebels JL, Roth WT, Kopell BS (1978) Cortical slow potentials and the occipital EEG in congenital blindness. J Neurol Sci 37:51-58.

Olavarria JF, Hiroi R (2003) Retinal influences specify cortico-cortical maps by postnatal day six in rats and mice. J Comp Neurol 459:156-172.

Pelli DG (1997) The VideoToolbox software for visual psychophysics: Transforming numbers into movies. Spat Vis 10:437-442.

Reimer J, Froudarakis E, Cadwell CR, Yatsenko D, Denfield GH, Tolias AS (2014) Pupil fluctuations track fast switching of cortical states during quiet wakefulness. Neuron 84:355-362.

Renart A, de la Rocha J, Bartho P, Hollender L, Parga N, Reyes A, Harris KD (2010) The asynchronous state in cortical circuits. Science 327:587-590.

Ribic A (2020) Stability in the face of change: Lifelong experience-dependent plasticity in the sensory cortex. Front Cell Neurosci 0:.

Riyahi P, Phillips MA, Colonnese MT (2021) Input-independent homeostasis of developing thalamocortical activity. eNeuro 8:10.1523/ENEURO.0184-Jun.

Röder B, Kekunnaya R (2022) Effects of early visual deprivation.

Seabrook TA, El-Danaf RN, Krahe TE, Fox MA, Guido W (2013) Retinal input regulates the timing of corticogeniculate innervation. J Neurosci 33:10085-10097.

Senzai Y, Fernandez-Ruiz A, Buzsáki G (2019) Layer-specific physiological features and

interlaminar interactions in the primary visual cortex of the mouse. Neuron 101:500-513.e5.

Shen J, Colonnese MT (2016) Development of activity in the mouse visual cortex. J Neurosci 36:12259-12275.

Shinomoto S et al (2009) Relating neuronal firing patterns to functional differentiation of cerebral cortex. PLoS Comput Biol 5:e1000433.

Torrado Pacheco A, Bottorff J, Gao Y, Turrigiano GG (2021) Sleep promotes downward firing rate homeostasis. Neuron 109:530-544.e6.

Turrigiano GG (2017) The dialectic of hebb and homeostasis. Philos Trans R Soc Lond B Biol Sci 372:10.1098/rstb.2016.0258.

Uhlhaas PJ, Haenschel C, Nikolić D, Singer W (2008) The role of oscillations and synchrony in cortical networks and their putative relevance for the pathophysiology of schizophrenia. Schizophr Bull 34:927-943.

Vinck M, Batista-Brito R, Knoblich U, Cardin JA (2015) Arousal and locomotion make distinct contributions to cortical activity patterns and visual encoding. Neuron 86:740-754.

Wu YK, Hengen KB, Turrigiano GG, Gjorgjieva J (2020) Homeostatic mechanisms regulate distinct aspects of cortical circuit dynamics. Proc Natl Acad Sci U S A 117:24514-24525.

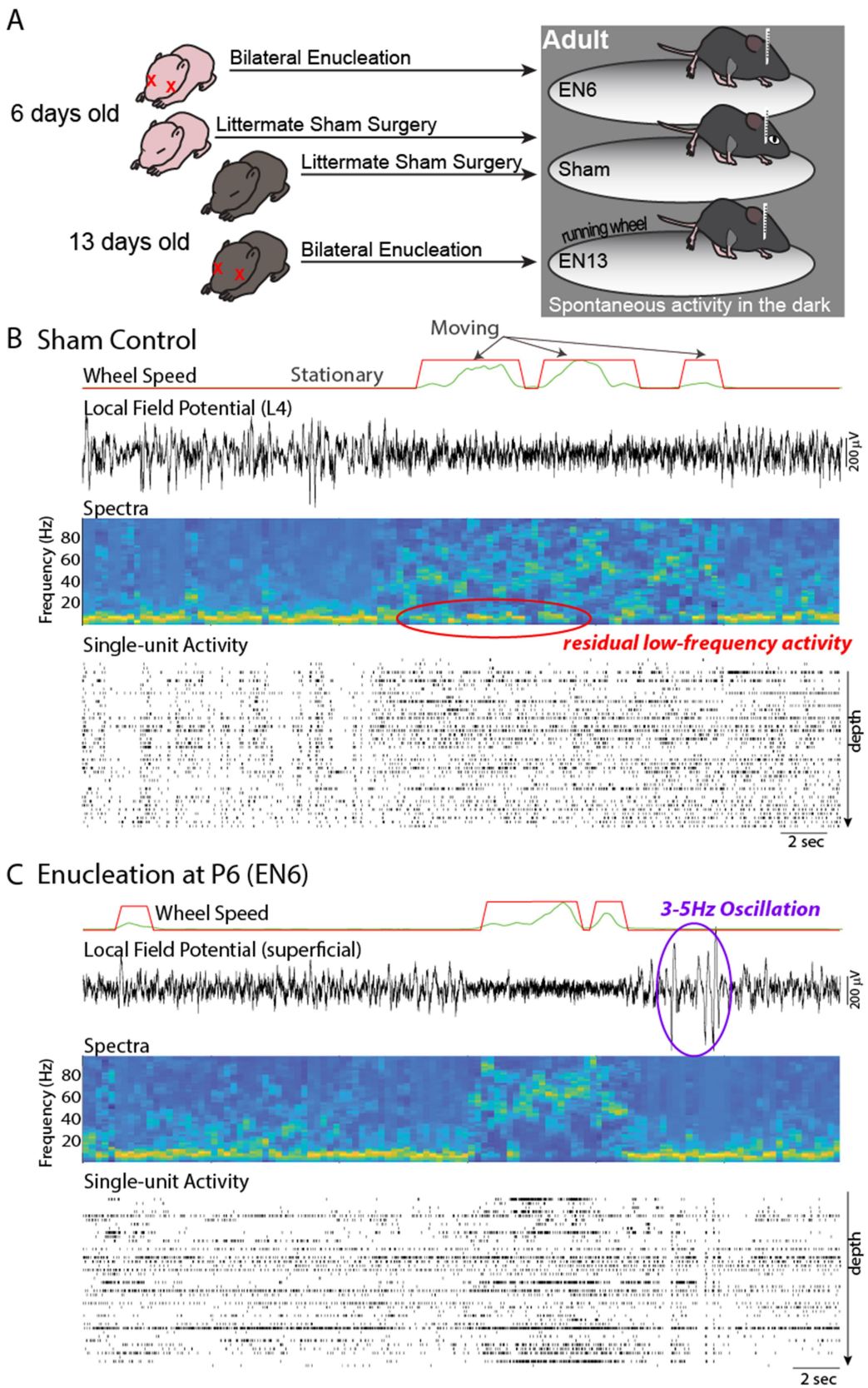
A
6 days old
13 days old
Bilateral Enucleation
Littermate Sham Surgery
Littermate Sham Surgery
Bilateral Enucleation
Adult
EN6
Sham
running wheel
EN13
Spontaneous activity in the dark
B Sham Control
Moving
Wheel Speed
Stationary
Local Field Potential (L4)
200 µV
Spectra
Frequency (Hz)
80
60
40
20
Single-unit Activity
residual low-frequency activity
depth
2 sec
C Enucleation at P6 (EN6)
Wheel Speed
3-5Hz Oscillation
Local Field Potential (superficial)
200 µV
Spectra
Frequency (Hz)
80
60
40
20
Single-unit Activity
depth
2 sec

Figure 1

Figure 1. Effect of bilateral enucleation on cortical dynamics. A. Experimental design. Mouse pups underwent bilateral enucleation at 6 days old (EN6), before the development of continuous background activity and adult-like cortical states, or at 13 days old (EN13), before eye-opening but after the initial emergence of background cortical activity and states(Shen and Colonnese, 2016; Riyahi et al., 2021). Littermates of each group received sham surgery and were recorded on interleaved days. Activity in the monocular visual cortex was recorded in adult head-fixed, awake animals allowed free movement on a circular treadmill in the dark. **B.** Representative recording from sham control littermate. Aligned time-courses show running disk velocity (green) and binarized threshold (red) dividing session into Stationary and Moving periods; local field potential (LFP) from layer 4, spectral decomposition of LFP signal on log(power) color scale; and raster plot of isolated single-unit firing arranged from surface at the top to layer 5 below. Red circle marks periods of residual low-frequency activity during moving periods which were observed to be absent in the enucleated animals. **C.** Representative recording from EN6 animal. Note qualitatively similar network dynamics including a decrease in EEG and unit synchronization and concomitant increase in firing during movement periods, while low-frequency activity is reduced during movement. Purple circle shows periods of large amplitude 3-5 Hz oscillations that occurred more frequently in the enucleated groups.

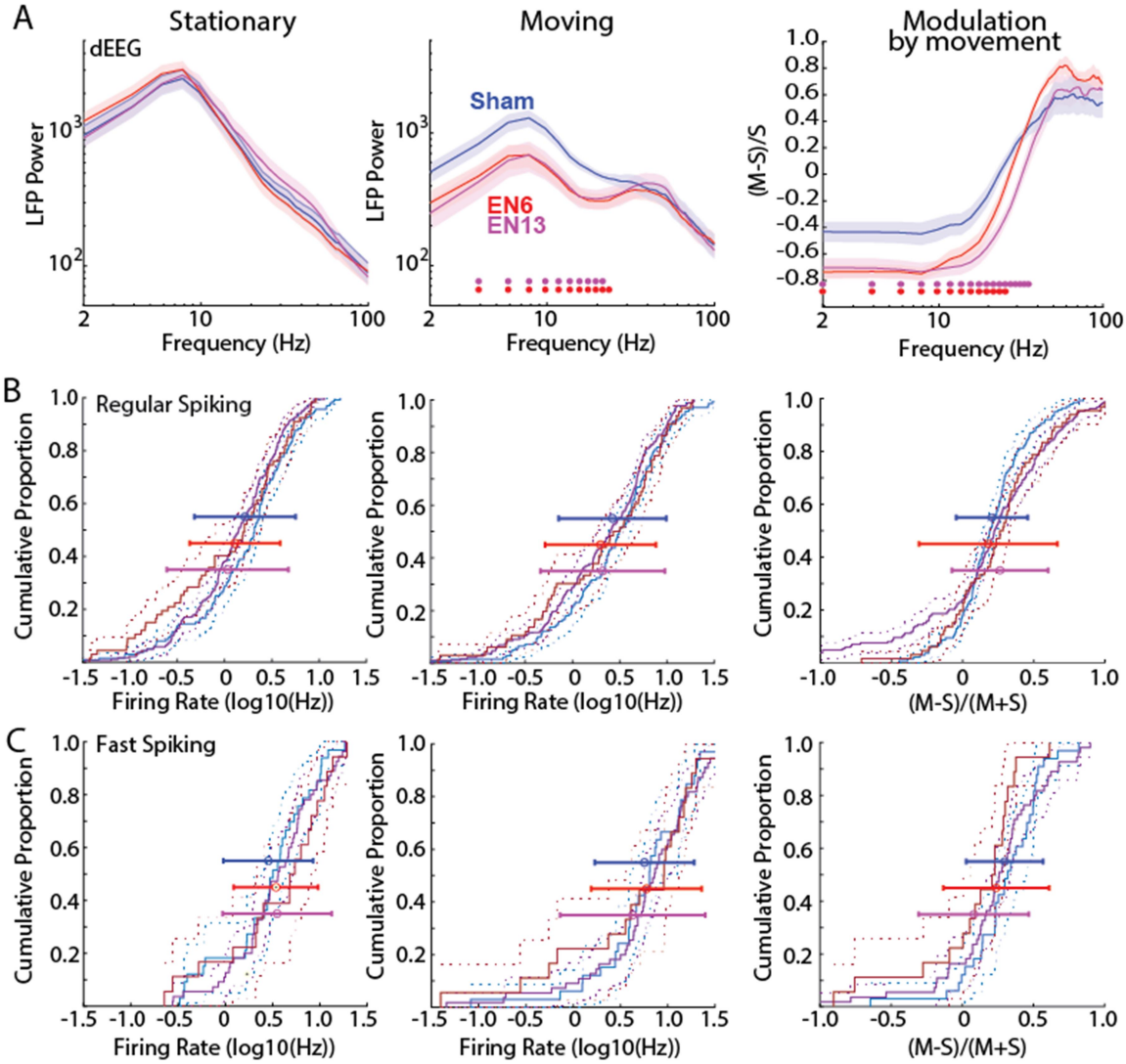

Figure 2. Effect of bilateral enucleation on EEG power and firing rates. A. Population mean and standard deviation for LFP power for Sham (blue), P6 enucleated(EN6; red) and P13 enucleated(EN13; purple). Power during periods of Stationary (left) and Moving (middle) periods and the proportional change during movement(Modulation by movement, right) are shown, with frequencies of significant difference(permutation test) from Sham shown by color coded dot for each experimental group. **B.** Cumulative distribution of single-unit firing-rates for regular spiking (presumptive excitatory) neurons during Stationary and Moving periods and for the modulation by movement. Solid lines show distribution and dotted lines the associated 95% confidence interval. Error bars show population mean and standard deviation for all neurons. Firing rates were not significantly different for any group (Table 1). **C.** Cumulative distribution for fast-spiking (presumptive inhibitory) neuron firing-rates.

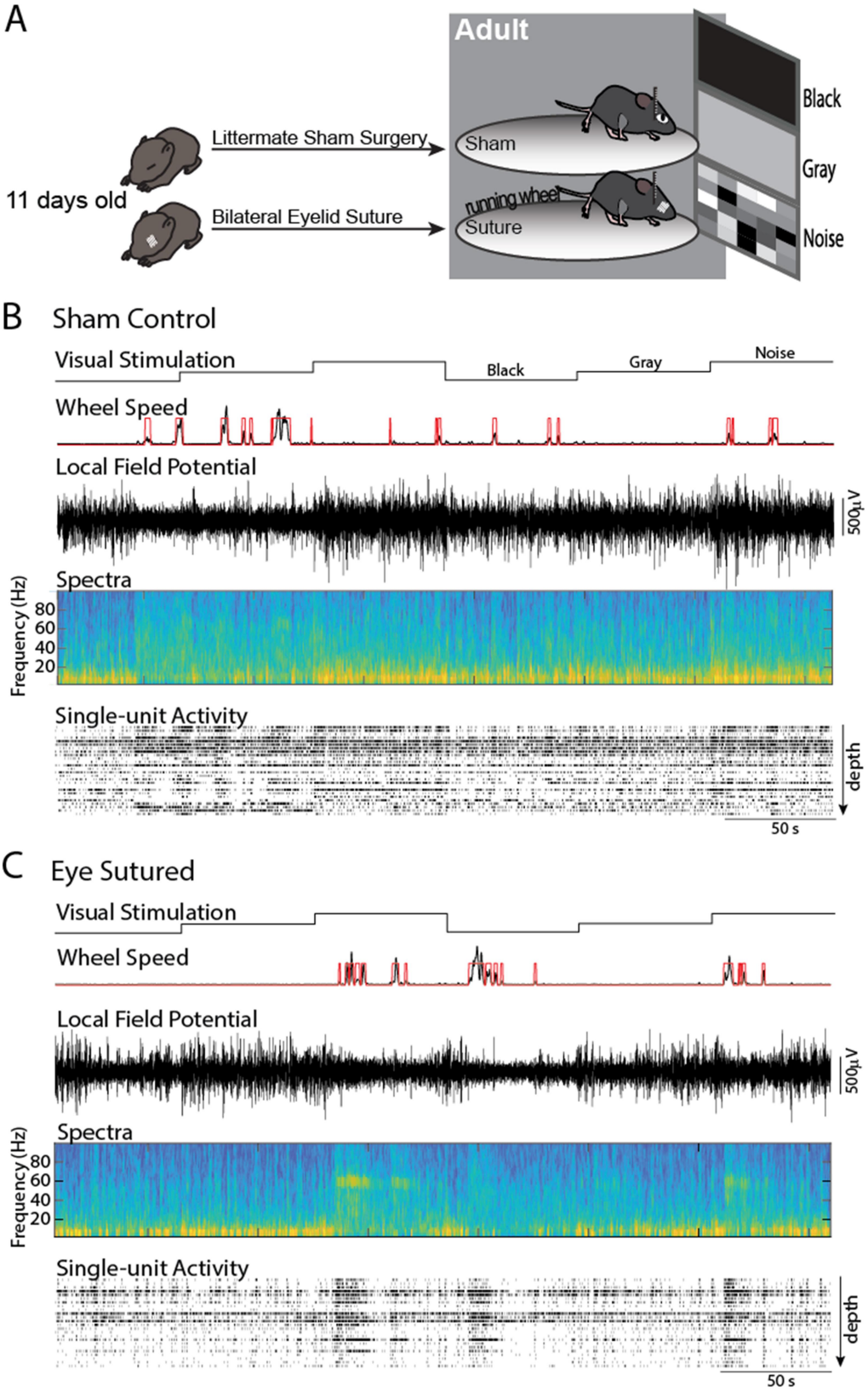
A
Adult
Black
Gray
Noise
Littermate Sham Surgery
Sham
11 days old
Bilateral Eyelid Suture
running wheel
Suture
B
Sham Control
Visual Stimulation
Black
Gray
Noise
Wheel Speed
Local Field Potential
500µV
Spectra
Frequency (Hz)
80
60
40
20
Single-unit Activity
depth
50 s
C
Eye Sutured
Visual Stimulation
Wheel Speed
Local Field Potential
500µV
Spectra
Frequency (Hz)
80
60
40
20
Single-unit Activity
depth
50 s

Figure 3

Figure 3. Effect of bilateral eyelid suture on cortical dynamics. A. Experimental design. Mouse pups underwent bilateral eyelid suture before natural eye-opening. Control littermates underwent sham surgery and were recorded on alternating days. Activity in the monocular visual cortex was recorded in adult head-fixed, awake animals allowed free movement on a circular treadmill while alternating blocks of visual stimuli were presented to the contralateral eye. Visual stimuli consisted of 1 min blocks of a ‘Black’ screen (full darkness), ‘Gray’ screen' or isoluminant ‘Noise’ stimuli of changing luminance blocks. **B.** Representative recording from a sham sutured animal across two rounds of stimulation. **C.** Representative recording from eye sutured littermate. Note qualitative similarity in state regulation between sham and sutured animals, including desynchronization of LFP and increased firing during movement. Also note the increased narrow band gamma generated by this eye-sutured animal during noise stimulation that was amplified by movement.

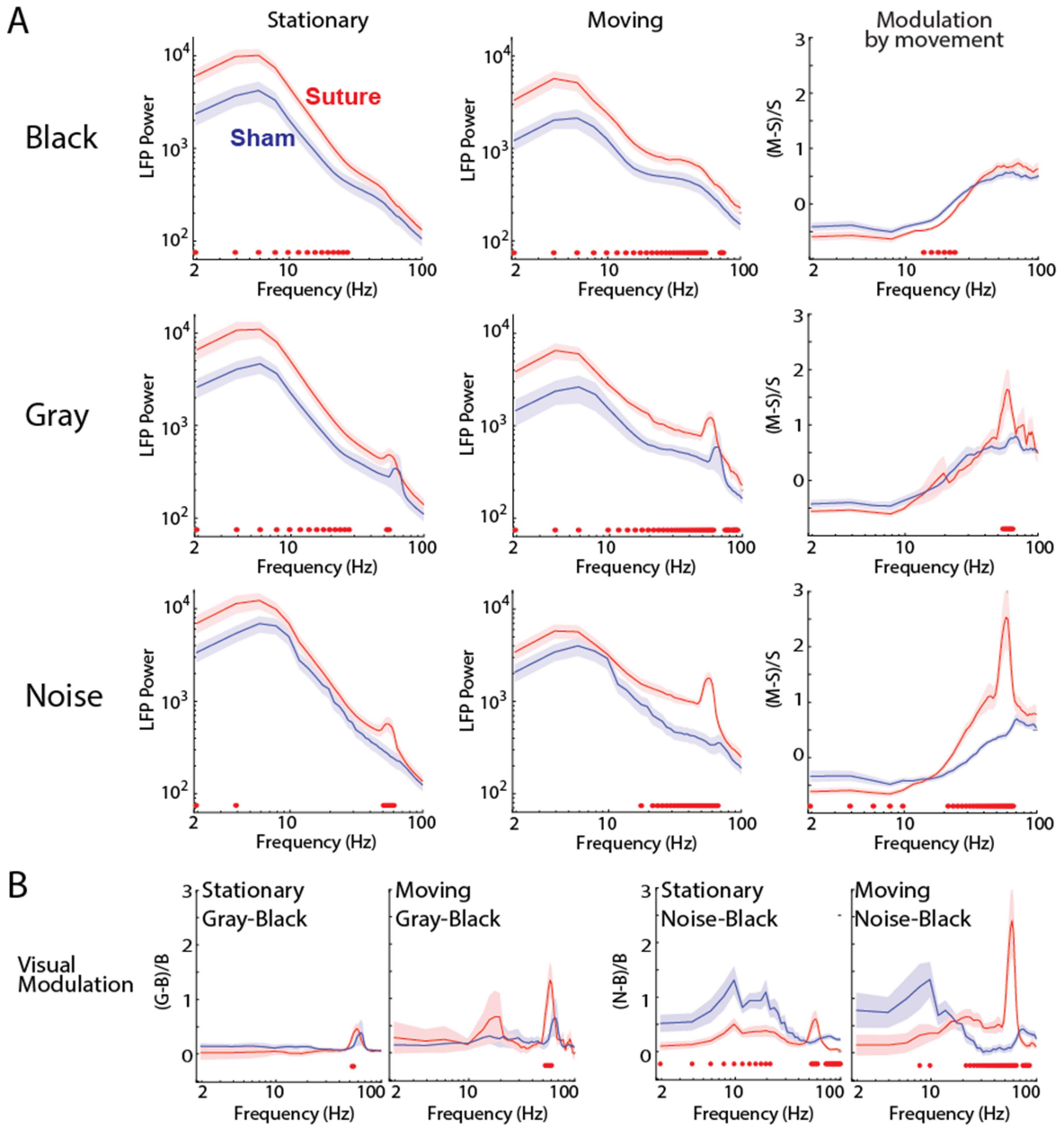

Figure 4. Effect of bilateral eyelid suture on EEG dynamics. A. Population mean and standard deviation of LFP frequency power by visual stimulation (row) and movement state (column). The far right column shows proportional change in power during movement. Frequencies statistically different between groups are marked by purple dots near the x-axis. **B.** Frequency-power change by visual stimulation for each movement condition. Power change for Gray screen(left two) and Noise stimulation(right two) relative to Black screen for Stationary and Moving conditions.

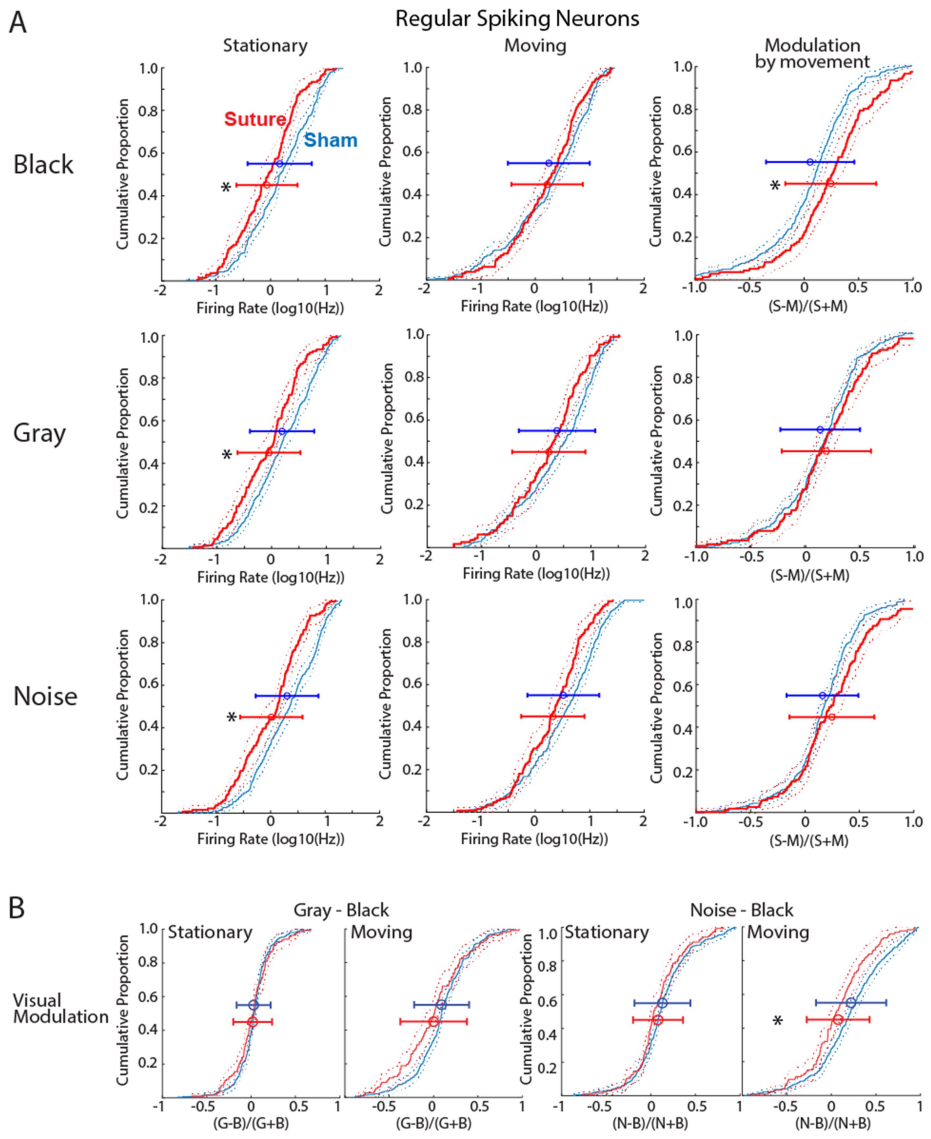

Figure 5. Effect of bilateral eyelid suture on regular spiking neuron firing-rates. A. Cumulative distribution histogram of regular spiking neuron firing rates by visual stimulus(row) and movement state(column). Change in firing rate by movement is shown in the right column. Solid lines show distribution and dotted lines the 95% confidence interval. Mean and standard deviation of each distribution is shown by the error bars. Significant difference(ANOVA post-hoc) between groups is shown by asterisk. Firing rates are lower for all stimulus conditions when the animals are stationary, but similar during movement. A significant difference for modulation by movement was observed only in the dark condition. **B.** Cumulative distribution of firing-rate modulation by visual stimulus, divided by behavioral state. Firing rate change relative to black screen is shown for gray screen(left two) and noise(right two) for each Stationary and Moving conditions. See Table 2 for associated data.

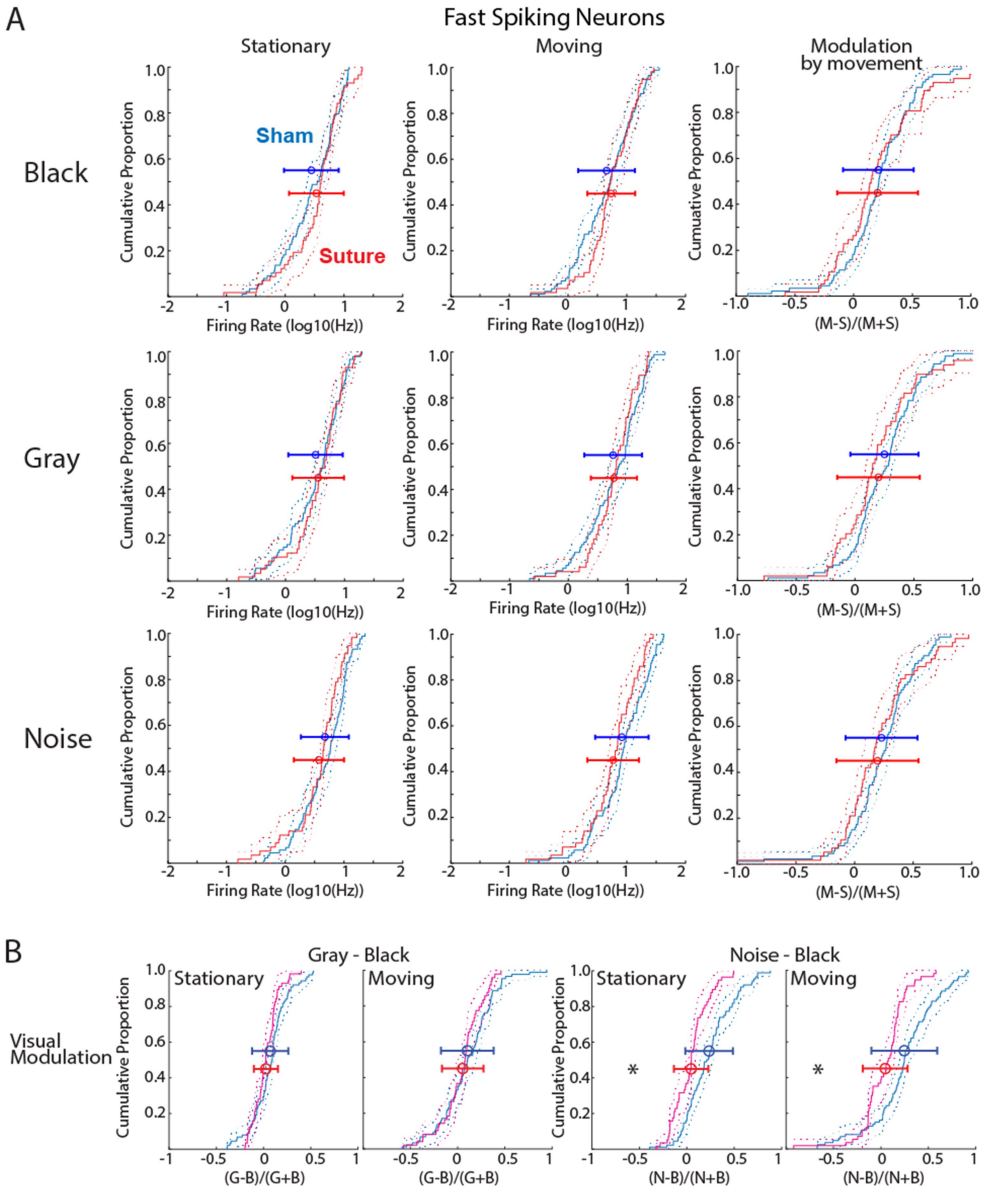

Figure 6. Effect of bilateral eyelid suture on fast spiking neuron firing-rates. A. Cumulative distribution histogram of fast-spiking neuron firing rates by visual stimulus(row) and movement state (column). Change in firing rate by movement is shown in the right column. Solid lines show distribution and dotted lines the 95% confidence interval. Mean and standard deviation of each distribution is shown by the error bars. No significant differences were found between groups for any condition. **B.** Cumulative distribution of firing-rate modulation by visual stimulus, divided by behavioral state. Firing rate change relative to black screen is shown for gray screen(left two) and noise(right two) for each Stationary and Moving conditions. Significant difference(ANOVA post-hoc) between groups is shown by asterisk. See Table 3 for associated data.

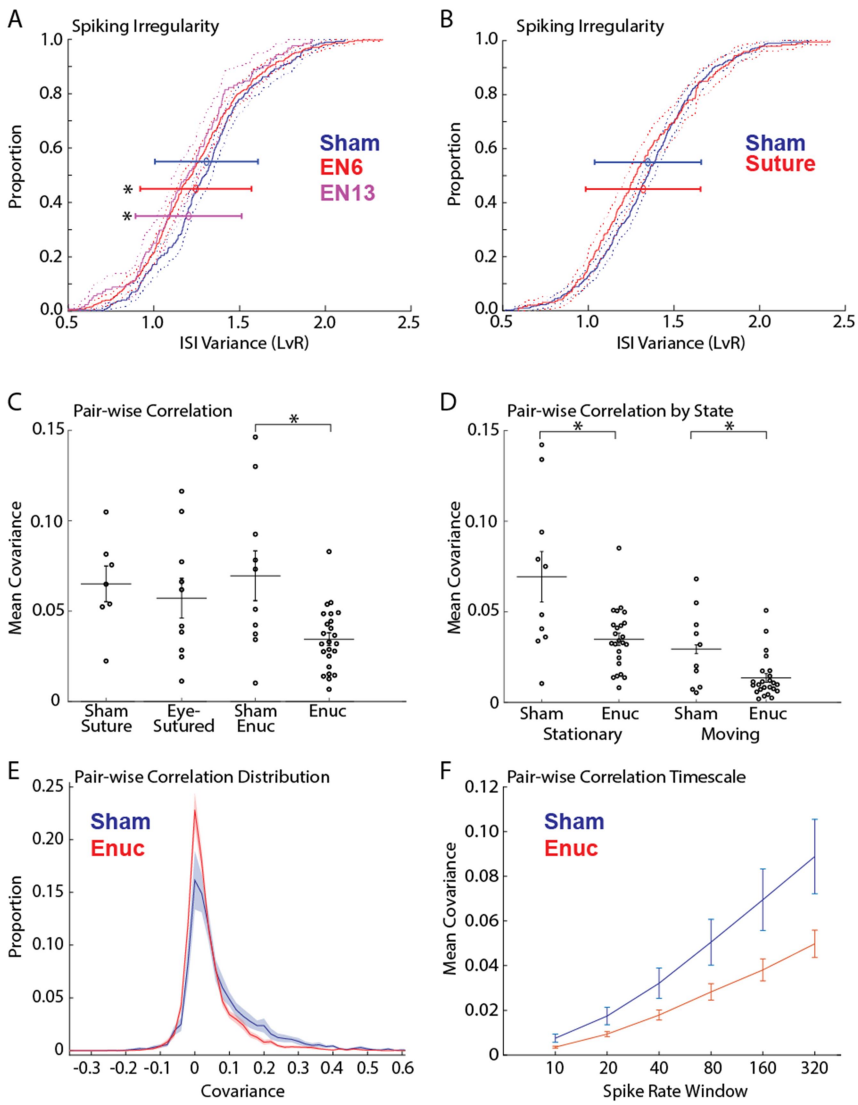

Figure 7. Effect of enucleation and eyelid suture on higher-order firing behavior. A. Cumulative distributions of spiking irregularity for the enucleation experiment. LvR is a normalized measure of interspike interval(ISI) that is not affected by firing rate(Shinomoto et al., 2009); higher LvR indicates less regular firing. Solid lines show distribution, dotted lines 95% confidence interval. Error bars show mean and standard deviation for each group. Significant difference from the Sham group(ANOVA post-hoc) is shown by asterisk. **B.** Cumulative distributions of spiking irregularity for the suturing experiment. **C.** Animal mean pairwise spike rate covariance for both experiments. Mean and standard deviation are shown along with each animal mean covariance measured for a 160 ms window. Asterisk shows significant difference from group control by ANOVA post-hoc. Both P6 and P13 enucleation groups were pooled. **D.** Population mean pairwise spike rate for enucleated groups for Stationary and Moving periods separately(160ms window). Asterisk shows significant difference from group control by ANOVA post-hoc. Reduced correlations caused by enucleation are present for both movement and Stationary periods. **E.** Distribution of pairwise correlations for all neurons(160ms window). Mean and standard deviation(shaded region) shown. **F.** Mean pairwise correlation by window size.

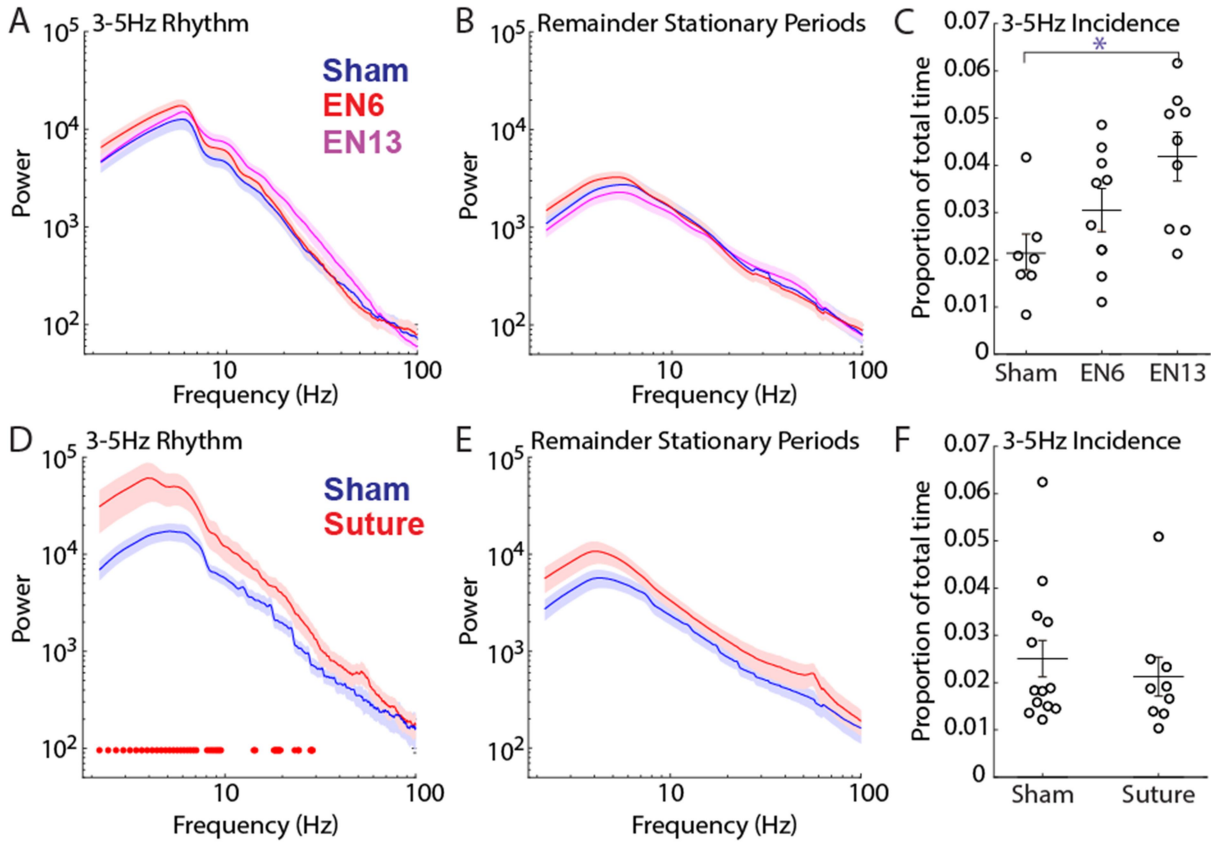

Figure 8. Effect of enucleation and eyelid suture on the 3-5 Hz, presumptive mouse alpha, rhythm. A. LFP frequency power for isolated periods of 3-5 Hz rhythm for the enucleation experiments. Population mean and standard deviation(shaded regions) is shown. No significant differences were observed for any frequency. **B.** LFP power for remainder of Stationary periods after removal of 3-5Hz periods. **C.** Proportion of time spent in 3-5Hz rhythm for each animal and the population mean and standard deviation. Significant difference(ANOVA post-hoc) is shown by asterisk. **D-F.** As for A-C with suture experiment. Significant difference between specific frequencies is shown by red dots near x-axis in D.

Regular Spiking Neurons

Firing Rates

Means and Standard Deviation

	Stationary	Moving
Open	0.22 ± 0.54	0.42 ± 0.57
EN06	0.11 ± 0.48	0.30 ± 0.59
EN13	0.03 ± 0.64	0.32 ± 0.66

ANOVA

Effect	F	p
Group	4.45	0.012
Move	26.39	<.00001
G*M	0.38	0.681

Post-hoc test

	OS	OM	6S	6M	13S	13M
OS						
OM	x					
6S		x				
6M			x			
13S		x		x		
13M					x	

Movement Modulation

Means and Standard Deviations

	Move-Stationary
Open	0.21 ± 0.25
EN06	0.18 ± 0.49
EN13	0.26 ± 0.34

ANOVA

Effect	F	p
Group	1.10	0.334

Fast Spiking Neurons

Firing Rates

Means and Standard Deviation

	Stationary	Moving
Open	0.45 ± 0.47	0.75 ± 0.53
EN06	0.54 ± 0.45	0.77 ± 0.58
EN13	0.55 ± 0.58	0.63 ± 0.77

ANOVA

Effect	F	p
Group	0.30	0.740
Move	6.20	0.014
G*M	0.47	0.624

Post-hoc test

	OS	OM	6S	6M	13S	13M
OS						
OM						
6S						
6M						
13S						
13M						

Movement Modulation

Means and Standard Deviations

	Move-Stationary
Open	0.30 ± 0.27
EN06	0.24 ± 0.37
EN13	0.08 ± 0.39

ANOVA

Effect	F	p
Group	2.32	0.104

Table 1. Single-Unit firing-rates following enucleation. Means and standard deviations, two-factor ANOVA and post-hoc test results for data displayed in **Fig. 2**. “Open” designates the Sham enucleated animals. For the ANOVA G*M shows the interaction between Group and Movement state. The post-hoc test results show $p<0.05$ by Tukey HSD, O/6/13 denote treatment group, S/M denote movement state (**S**tationary/**M**oving).

Regular Spiking Neurons

Firing Rates

Means and Standard Deviations

		Black	Gray	Noise
Stationary	**Open**	0.17 ± 0.59	0.19 ± 0.59	0.30 ± 0.58
	Sutured	-0.07 ± 0.56	-0.05 ± 0.58	0.01 ± 0.57
Moving	**Open**	0.25 ± 0.75	0.38 ± 0.70	0.51 ± 0.66
	Sutured	0.22 ± 0.66	0.23 ± 0.67	0.32 ± 0.58

ANOVA

Effect	F	p
Group	48.06	<.00001
Move	68.42	<.00001
Stim	10.12	<.00001
G*M	5.84	0.016
G*S	1.33	0.264
M*S	0.69	0.499
G*M*S	0.44	0.646

Post-hoc test

	OSD	OSG	OSN	OMD	OMG	OMN	SSD	SSG	SSN	SMD	SMG
OSD											
OSG											
OSN											
OMD											
OMG	x	x									
OMN	x	x	x	x							
SSD	x	x	x	x	x	x					
SSG	x	x	x	x	x	x					
SSN			x	x	x	x					
SMD						x	x	x			
SMG						x	x	x			
SMN							x	x	x		

Movement Modulation

Means and Standard Deviations

	Black	Gray	Noise
Open	0.05 ± 0.41	0.14 ± 0.36	0.17 ± 0.33
Sutured	0.24 ± 0.42	0.20 ± 0.41	0.25 ± 0.39

ANOVA

Effect	F	p
Group	21.83	<.00001
Stim	2.41	0.090
G*S	2.97	0.052

Post-hoc test

	OD	OG	ON	SD	SG
OD					
OG					
ON	x				
SD	x				
SG	x				
SN	x				

Visual Stimulation Modulation

Means and Standard Deviations

		Gray-Black	Noise-Black
Stationary	**Open**	0.03 ± 0.19	0.13 ± 0.31
	Sutured	0.02 ± 0.22	0.08 ± 0.28
Moving	**Open**	0.09 ± 0.31	0.22 ± 0.39
	Sutured	0.00 ± 0.38	0.08 ± 0.35

ANOVA

Effect	F	p
Group	20.01	<.00001
Move	4.03	0.045
Stim	31.41	<.00001
G*M	7.17	0.008
G*S	1.96	0.162
M*S	0.41	0.520
G*M*S	0.07	0.798

Post-hoc test

	OSG	OSN	OMG	OMN	SSG	SSN	SMG
OSG							
OSN	x						
OMG							
OMN	x	x	x				
SSG		x		x			
SSN				x			
SMG		x		x			
SMN				x			

Table 2. Single-Unit regular-spiking neuron firing-rates following eyelid suture. Means and standard deviations, two-factor ANOVA and post-hoc test results for data displayed in **Fig. 5**. “Open” designates the Sham sutured animals. For means, red indicates significant difference from sham group (by Post-hoc test). For the ANOVA ***** shows the interaction between factors (eg. **G*M** is the Group ***** Movement interaction). The post-hoc test results show $p<0.05$ by Tukey HSD. For the top and bottom charts the first letter (O/S) denotes treatment group; the second letter S/M denotes movement state (**S**tationary/**M**oving), the third letter D/G/N denotes stimulus block (Dark/Gray/Noise).

Fast Spiking Neurons

Firing Rates

Means and Standard Deviation

		Black	Gray	Noise
Stationary	**Sham**	0.45 ± 0.47	0.51 ± 0.46	0.68 ± 0.41
	Sutured	0.53 ± 0.47	0.55 ± 0.44	0.57 ± 0.43
Moving	**Sham**	0.66 ± 0.48	0.76 ± 0.49	0.92 ± 0.46
	Sutured	0.74 ± 0.41	0.77 ± 0.39	0.77 ± 0.44

ANOVA

Effect	F	p
Group	0.02	0.877
Move	49.02	<.00001
Stim	6.89	0.0011
G*M	0.02	0.663
G*S	3.96	0.020
M*S	0.07	0.936
G*M*S	0.03	0.967

Post-hoc test

	OSD	OSG	OSN	OMD	OMG	OMN	SSD	SSG	SSN	SMD	SMG
OSD											
OSG											
OSN	x										
OMD											
OMG	x	x									
OMN	x	x	x	x							
SSD						x					
SSG		x				x					
SSN						x					
SMD	x										
SMG	x	x									
SMN	x	x									

Movement Modulation

Means and Standard Deviations

		Black	Gray	Noise
	Open	0.21 ± 0.30	0.25 ± 0.29	0.23 ± 0.31
	Sutured	0.20 ± 0.34	0.20 ± 0.35	0.20 ± 0.35

ANOVA

Effect	F	p
Group	0.93	0.3353
Stim	0.10	0.906
G*S	0.17	0.848

Post-hoc test

	OD	OG	ON	CD	CG
OD					
OG					
ON					
CD					
CG					
CN					

Visual Stimulation Modulation

Means and Standard Deviations

		Gray-Black	Noise-Black
Stationary	**Open**	0.07 ± 0.19	0.23 ± 0.25
	Sutured	0.03 ± 0.13	0.05 ± 0.18
Moving	**Open**	0.10 ± 0.28	0.25 ± 0.35
	Sutured	0.05 ± 0.22	0.05 ± 0.24

ANOVA

Effect	F	p
Group	32.83	<.00001
Move	0.74	0.390
Stim	14.40	0.0002
G*M	0.04	0.847
G*S	12.06	0.001
M*S	0.34	0.559
G*M*S	0.01	0.925

Post-hoc test

	OSG	OSN	OMG	OMN	CSG	CSN	CMG
OSG							
OSN	x						
OMG		x					
OMN	x		x				
CSG		x		x			
CSN		x		x			
CMG		x		x			
CMN		x		x			

Table 3. Single-Unit fast-spiking neuron firing-rates following eyelid suture. Means and standard deviations, two-factor ANOVA and post-hoc test results for data displayed in **Fig. 6**. Abbreviations are the same as **Table 2**.